Construction and Building Materials 52 (2014) 221–226

Contents lists available at ScienceDirect

Construction and Building Materials

journal homepage: www.elsevier.com/locate/conbuildmat

Three-dimensional quantification of pore structure in coal ash-based geopolymer using conventional electron tomography

Sujeong Lee [a,*], Hyeong-Tae Jou [b], Arie van Riessen [c], William D.A. Rickard [c], Chul-Min Chon [a], Nam-Hee Kang [d]

[a] Mineral Resource Research Division, Korea Institute of Geoscience and Mineral Resources, Daejeon, South Korea
[b] Maritime Security Center, Korea Institute of Ocean Science and Technology, Ansan, South Korea
[c] Centre for Materials Research, Curtin University, Perth, Australia
[d] University of Science and Technology, Daejeon, South Korea

HIGHLIGHTS

- We report the pore structure of geopolymers at the nanoscale for the first time.
- The porosity is determined to be 7.15% for the volume of interest, 0.00748 μm^3.
- Most of the pores are not connected and have irregular geometry.
- The research results will contribute to understand the durability of geopolymers.

ARTICLE INFO

Article history:
Received 1 July 2013
Received in revised form 17 October 2013
Accepted 31 October 2013
Available online 5 December 2013

Keywords:
Geopolymer
Electron tomography
Porosity
Pore connectivity

ABSTRACT

X-ray tomography, mercury intrusion porosimetry, and gas adsorption are used to characterize the nano-scale pore structure of geopolymers with little success. This is because X-ray tomography still lacks high resolution for nanometer-sized pores and the other techniques use the incorrect assumptions of regular pore geometry and interconnected pore systems. To reveal the three-dimensional structure of nanometer-sized pores in coal ash-based geopolymer, conventional bright field electron tomography is used in this study for the first time. Because artifacts resulting from diffraction effects of newly-formed zeolite-like phases are introduced only in the matrix surrounding the pores, the pore size distribution has been investigated successfully. Most of the pores had irregular geometry and were found to range from 20 to 60 nm in equivalent perimeter diameter. The porosity was determined to be 7.15% for the volume of interest, 0.00748 μm^3. The first successful outcome of the reported experiment indicates that electron tomography will play an important role in the future for measuring the porosity and pore connectivity of geopolymers enabling predictions of durability and optimization of material properties.

1. Introduction

Geopolymers are a class of alkali-activated materials synthesized by the chemical reaction of aluminosilicate source materials with alkaline activating solutions near ambient temperatures [1]. Pozzolanic materials including fly ash, metakaolin and natural pozzolans are used as a feedstock for producing geopolymers [1]. It is widely accepted that silicon and aluminum in the feedstock are dissolved in an alkaline solution and a three-dimensional network structure subsequently hardens, although the geopolymerization process is not fully understood yet. Some performance advantages over ordinary Portland cement (OPC) which are only offered by geopolymers, such as corrosion resistance, fire resistance, high compressive and tensile strengths, and a rapid strength gain, enable geopolymers to become one of the potential alternatives to OPC, with significant reduction in CO_2 emissions. However, the issue of long term durability remains one of the obstacles to the commercialization of geopolymer cement for construction applications. In case of OPC, many serious studies have been carried out on the microstructure, pore structure and interface between aggregates and cement binder [2–8]. Pore volume, pore size distribution and pore connectivity affect many of the properties of binding materials such as permeability, shrinkage, elastic modulus and

* Corresponding author. Address: Korea Institute of Geoscience and Mineral Resources, 305-350 Daejeon, South Korea. Tel.: +82 42 868 3125; fax: +82 42 868 3418.
E-mail address: crystal2@kigam.re.kr (S. Lee).

0950-0618
http://dx.doi.org/10.1016/j.conbuildmat.2013.10.072

strength [9,10]. In addition, the long term durability is directly impacted by the porosity of geopolymers and OPC [11–13]. Duxson et al. asserts that the microstructures including pore volume, porosity and pore distribution around the gel framework determine the mechanical properties of the geopolymer, rather than simple compositional effects [14]. Geopolymers inevitably contain pores and penetration of external species such as chloride occurs through the pore network to degrade the geopolymer concrete. Therefore characterization and quantification of the pore structure in geopolymers are fundamental for understanding its influence on durability of geopolymers, formulating geopolymers for specific applications and producing geopolymers on a commercial scale.

Gas adsorption and mercury intrusion porosimetry (MIP) are widely used for determining pore size distribution. However, the data interpretation of these techniques is based on assumptions of regular pore geometry and an interconnected pore system in the materials [10,15]. In fact the use of MIP for cement and concrete has been strongly criticized [15] and Lange et al. [16] claims that pore sizes may be up to three orders of magnitude lower than those obtained by SEM images [16]. In addition, some voids in the geopolymers are disconnected and bounded by the gel in the backscattered electron images [13]. X-ray microtomography has been used to obtain information about the pore size distribution in Portland cement products because it is non-destructive and direct visualization of the pore structure is possible [9,11,12]. X-ray tomography has also been used to evaluate pore structure of geopolymers [17,18]. Studies by Provis et al. show that unreacted fly ash particles are bound to geopolymer gel but the results are not able to provide clear three-dimensional views of pore structure due to limited resolution [17,18]. The impact of constrained resolution with X-ray tomography is that pore volume is severely underestimated based on a lower pore size range of 100–400 nm [17,18]. For all these reasons characterizing pore structure in geopolymers is considered very challenging.

Electron tomography is a widely-adopted imaging technique for the three-dimensional structural characterization of materials at nanometer-scale resolution [19,20]. The two basic steps of electron tomography are the acquisition of projection images, which are acquired by tilting the specimen holder, and calculation of the three dimensional reconstruction of the sample volume from these projections [19]. The resolution of electron tomography is between that of atom probe tomography (atomic) and X-ray microtomography (μm) [19].

The purpose of this article is to quantify the nanopore network structure of coal ash-based geopolymer by conventional electron tomography in order to better understand the nanometer-scale pore structure, which has seldom been reported. The first successful outcome of three-dimensional reconstruction from electron micrographs will trigger an understanding of the porosity and pore connectivity of geopolymers, enabling predictions of permeability and durability.

2. Experimental procedure

2.1. Characterization of coal ash

The geopolymer samples used in this study were synthesized from a pond ash which is mainly bottom ash mixed with a small amount of coarse rejected fly ash produced in Samcheonpo power station in South Korea. Bottom ash is coarse porous ash particle and gray–brown colored. Rejected fly ash is a coarse fraction of fly ash which is dumped in ash ponds due to its high carbon residue content and large particle size (usually >45 μm) [21]. The coal ash was collected from the ash pond and dried for 3 days at room temperature. Then it was crushed and pulverized to a fineness of 43% passing 65 mesh (212 μm). A 500 g lot of the crushed ash was slurried in 500 ml of water and wet ground in a rod mill to a particle size of less than 212 μm. Carbon residue content was determined by means of a proximate analysis. Carbon residue, on account of its hindrance of geopolymerization [22–24], was removed by froth flotation. About 60 g/t of collector (kerosene) and 20 g/t of frother (pine oil) were used to adsorbing selectively onto the surfaces of particles and rendering the froth stable enough without losing the attached carbon particles. About 600 g/t of dispersing agent (Na_2SiO_3) was used for minimizing heterocoagulation and promoting selectivity. The flotation circuit consisted of one stage of roughing and two stages of scavenging. After the froth flotation stages, the cleaned ash was dewatered and dried in an oven for 1 day for the use as a feedstock for producing geopolymers. The carbon content of the cleaned ash was measured by means of a proximate analysis.

Chemical analysis was carried out with an X-ray fluorescence spectrometer (Model: MXF-2100, Shimadzu, Japan). For quantitative phase analysis by X-ray diffraction analysis, 3.0000 g of the cleaned coal ash sample was thoroughly mixed with 8 ml of laboratory grade ethanol and 0.3333 g of an internal standard, fluorite (CaF_2 99.985%, Alfa Aesar, US) by milling for 5 min in a McCrone micronising mill. The reactive component was determined using XRF and quantitative XRD (D8 Advance and TOPAS 4.2, Bruker, Germany) using the same approach including Rietveld quantitative phase analysis and determination of amorphous composition described by Williams and van Riessen [25]. The same method of formulating geopolymer, as developed by Williams and van Riessen [25], was used, but the water content, which is the sum of water in alkali activators and free water, was additionally constrained by 22% of the mix weight.

2.2. Geopolymer synthesis and test procedure

Sodium silicate solution (SiO_2 36.50%, Na_2O = 18.00%, Kanto Chemical Co., Inc.) and sodium hydroxide (Wako Pure Chemical Industries, Ltd.) were used as the activators in order to achieve a Si:Al ratio of 2.0 and Na:Al ratio of 1.2 in the geopolymer binder. The geopolymer samples were formed by mixing ash and activators for 15 min in a laboratory cement mixer. The resulting paste was placed in 5 cm cube molds, sealed and cured at 70 °C for 24 h prior to demolding. The 1 day compressive strength of the paste was determined to be 49.8 MPa based on the average of three samples with a standard deviation of 4.7 MPa.

2.3. TEM Data acquisition and image processing

The geopolymer lamella was prepared by focused ion beam milling (Focused Ion Beam, Quanta 3D FEG, FEI) from a region that was identified as geopolymer gel and was relatively free of unreacted precursor ash. The cutting was done with gallium ions at 30 kV and 15 nA followed by final thinning at 5 keV and 48 pA to minimize the presence of milling artifacts. Gold colloid solution (protein A conjugated with colloidal gold, Utrecht University, The Netherlands) was diluted 10 times with distilled water to use ten-nanometer gold particles as fiducial markers to facilitate precise alignment of the tilt series. To place gold nanoparticles on the specimen, the lamella was soaked in diluted gold colloid solution for 1 min and then taken out for drying. Gold particles sat on both surfaces of the specimen. TEM imaging was performed using a FEI TECNAI G^2 Spirit equipped with a large tilt-angle holder and a 2048 × 2048 pixel CCD camera for image acquisition. Bright field (120 keV accelerating potential) tilt series images of the lamella were obtained from −55° to +55° at an interval of 1° of the tilt angle. The accurate alignment of the tilt series is an essential stage in electron tomography. New model formula, modified from Diez et al. [26], was used for the alignment of tilt series. This is based on previous research on the improved accuracy of alignment of projection images [27]. Three dimensional reconstruction of the TEM images was performed by the widely used filtered back-projection method [28]. The size of each image was reduced to half its size by averaging pixels, namely 1024 pixel by 1024 pixels, for minimizing the computational load. Reconstructed tomograms were viewed and analyzed using Chimera software v.1.6 (University of California, San Francisco, USA) and IMOD v. 4.1.10.

3. Results and discussion

3.1. Characterization of coal ash

The collected pond ash showed a wide range of particle sizes and shapes (Fig. 1(a)). Bottom ash particles are characterized by their large particle size, porous and sandy shape, and brown–gray color[1] (Fig. 1(b)). Most of ash particles were aluminosilicate phases with small amount of iron, calcium, potassium, magnesium and sodium (Fig. 1(c)). The chemical composition of the cleaned pond ash as determined by XRF is shown in Table 1. It mainly consists of silica (57.7%), alumina (22.6%) and iron (9.70%). It contains only 4.13% of CaO, which means it falls under ASTM C618 Class F fly ash based on chemical composition. The content of carbon residue was

[1] For interpretation of color in Fig. 1, the reader is referred to the web version of this article.

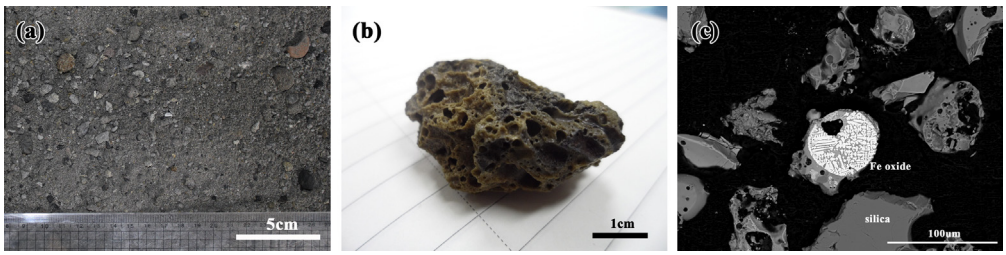

Fig. 1. (a) As-collected pond ash of Samcheonpo power station and, (b) a coarse porous and sandy lightweight bottom ash particle and (c) Backscattered electron image showing iron oxide phase formed inside aluminosilicate phase and discrete silica particle. All but silica and aluminosilicate phase particles embedding iron oxide are aluminosilicate phase with small amount of iron, calcium, potassium, magnesium and sodium.

Table 1
Chemical composition of the cleaned pond ash from Samcheonpo power station (wt%).

SiO_2	Al_2O_3	Fe_2O_3	CaO	MgO	K_2O	Na_2O	TiO_2	MnO	P_2O_5	Ig loss
57.7	22.6	9.70	4.13	1.48	1.47	0.68	1.12	0.13	0.32	0.39

determined to be 4.69%. Carbon was not detected in the cleaned ash fraction by means of a proximate analysis.

The Rietveld quantitative phase analysis result in Fig. 2 shows that the major crystalline phases of the ash include quartz (16.1 wt%), mullite (15.5 wt%), albite (7.4 wt%) and hematite (1.5 wt%). The amorphous fraction was 59.5 wt% and the composition of the amorphous fraction was calculated from the difference between the bulk chemical composition and the crystalline components as oxides (Table 2). The Si:Al ratio of the reactive component of the cleaned coal ash was determined to be 1.30. Therefore silicon and sodium must be added to the ash to achieve a Si/Al ratio of 2.0 and Na/Al ratio of 1.2. The mix proportion of the geopolymer gel was determined to be 61.5 wt% ash, 24.3 wt% silicate solution, 4.2 wt% NaOH and 10.0 wt% distilled water.

Table 2
Chemical composition of the amorphous fraction of the pond ash.

SiO_2	Al_2O_3	Fe_2O_3	CaO	MgO	K_2O	TiO_2	MnO	P_2O_5
25.9	17.1	8.30	4.20	1.50	1.50	1.10	0.10	0.30

3.2. Structure of nanometer-sized pores in geopolymer

The pore structure of the geopolymer lamella was clearly delineated by the high contrast between the paste and pores (Fig. 3). Also distinct were numerous dark spherical gold particles (fiducial markers) and many small crystals distinguishable due to Bragg scattering contrast in the tilt series. Crystalline phases are nearly always present in geopolymers though the gel phase is amorphous. The crystals were usually larger, darker and less symmetrical than the gold particles (Fig. 3). Diffuse diffraction rings arising from the gold particles were distinguished in electron diffraction analysis but no diffraction spots or rings were produced from the crystalline phase. Distinct spots or rings in the diffraction pattern reflect the degree of long-range order. On the other hand, disordered nanoparticles produce no visible diffraction spots or rings due to their extremely small size, thus resulting in crystallite size broadening, especially if the population of nanoparticles is small. Hence the crystalline phase was assumed to be a less ordered zeolite-like phase based on the energy dispersive X-ray spectroscopy data and conclusions reached by other researchers [29,30]. It is generally accepted that geopolymerization produces aluminosilicate gel phases with varying degrees of zeolite formation [31,32].

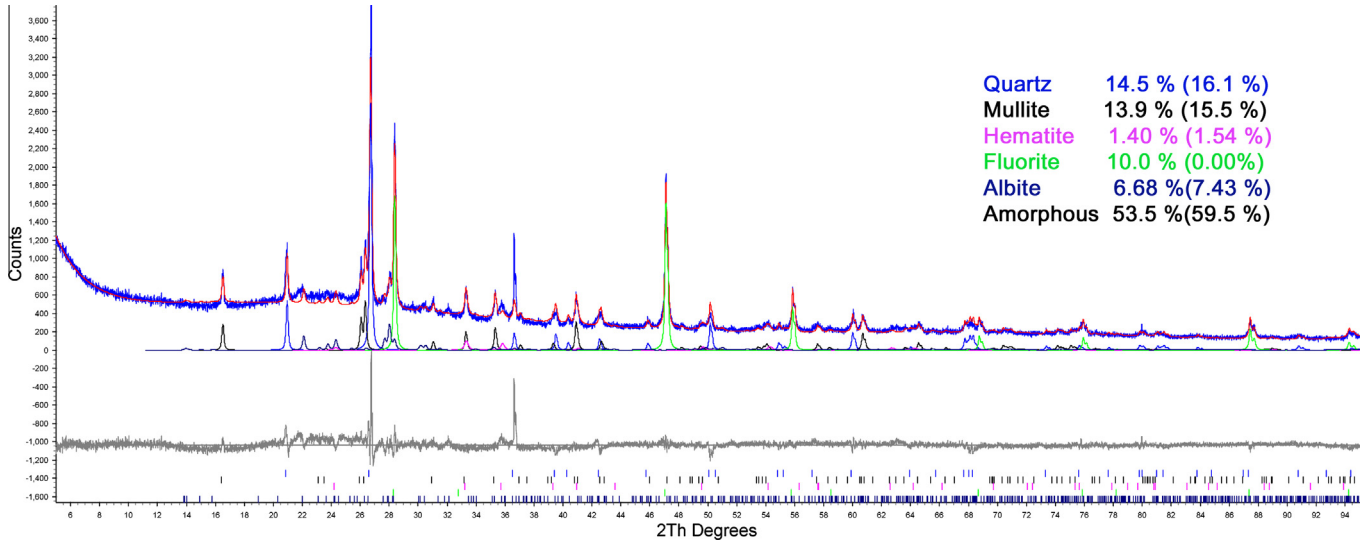

Fig. 2. Plot showing the observed and calculated powder X-ray diffraction patterns. The Bragg reflections for the phases are indicated by vertical bars.

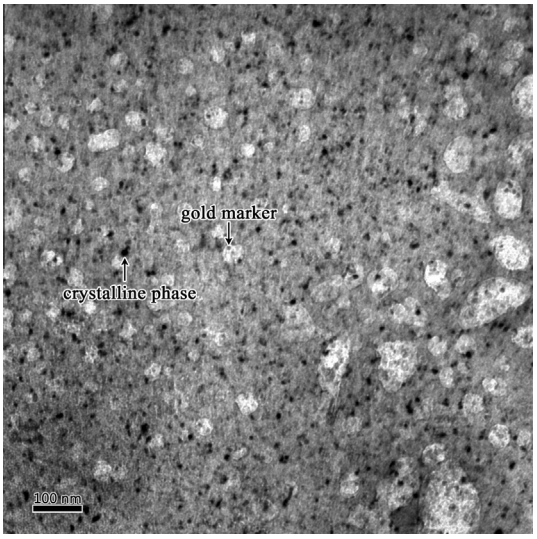

Fig. 3. TEM bright-field micrograph of the geopolymer lamella. Gold fiducial markers and numerous small crystals were observed as well as various sized pores.

Two z-slice images spaced about 10.7 nm apart are presented in Fig. 4. The equivalent perimeter diameters of some pores have been labeled in Fig. 4(a) and (b). The majority of pores seemed to be roughly spherical or oblate, but some were rather irregular in shape. The equivalent perimeter diameters of 145 pores in four different z-slices (including Fig. 4), each separated by 10.7 nm, were in the size range 13.5–147 nm (Fig. 5). The majority of pores were between 20 and 60 nm in diameter (Fig. 5) with eight falling outside this range, such as the elongated pore that was over 80 nm (circled in Fig. 4(b)). A number of the pores are likely present in two or more slices because the slices are only 10.7 nm apart. Thus the size range does not represent the diameters of 145 unique pores, but it certainly provides tangible approximations of pore size.

3.3. Porosity of geopolymer at the nanoscale

To extract quantitative data of porosity in a geopolymer, segmentation was carried out on the lower left quarter of the three dimensional reconstruction presented in Fig. 6. Segmentation is a process of grouping pixels based on different gray values to distinguish different phases; for instance the pore space from the gel in a geopolymer. It is generally performed manually, however the main limits of manual segmentation are that it is very time-consuming

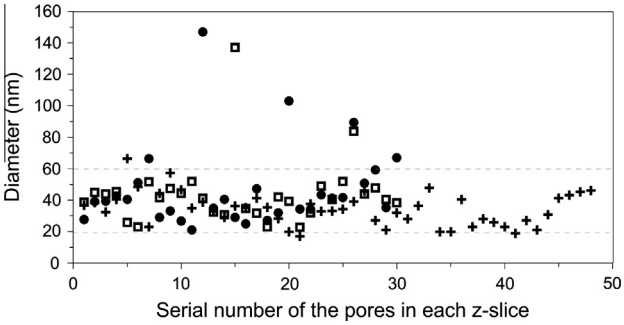

Fig. 5. Pore size distribution for the geopolymer represented by the diameters of the circumscribed circles of each pore in four z-slice images including those in Fig. 4. Pores from each z-slice are denoted with the same symbol.

and can be subjective [33]. Quantification based on segmentation by thresholding can segment the image into dissimilar phases rapidly [34], but the choice of threshold directly from the voxel intensity histogram is quite challenging and cannot be accurate due to the overlapping intensity distributions [18]. In many cases, the threshold is selected by visual perception to segment void, which is subjective, and results in attenuation of validity and reliability of the threshold method. In this case, manual segmentation can be the next alternative choice despite its limits. We quantified the porosity by manual segmentation because a threshold could not be selected to fully segment the pore and the gel in z-slices. Meanwhile, soaking the lamella in diluted gold colloid solution and followed drying process bent the lamella gently and reduced the available volume of interest for quantifying porosity. The width, length and thickness of the slab which was chosen for segmentation in the lower left quarter of the area shown in Fig. 3 were 482, 482, 32.2 nm and the volume of interest was 0.00748 μm^3, which corresponds to 19.3% of the three-dimensional reconstruction of 0.0387 μm^3. Porosity for this region was determined to be 7.15%. This value is much lower than 30.5% of Lloyd et al. [35] and about 23–38% Ma et al. [13], who studied spatial distribution of pores by Wood's metal intrusion porosimetry and MIP, respectively. This discrepancy might be related to different chemical properties of feedstocks, formulations, curing conditions, sample ages and, most of all, differences in resolutions and volumes of interest between porosity measurement equipments. Electron tomography provides insights into pore architecture for a very small volume at the nanometer level, with higher resolution than other porosity measurement methods such as MIP, metal intrusion porosimetry and X-ray tomography, which are used for big objects usually up to dozens of millimeters. Kriven et al. [36] and Duxson

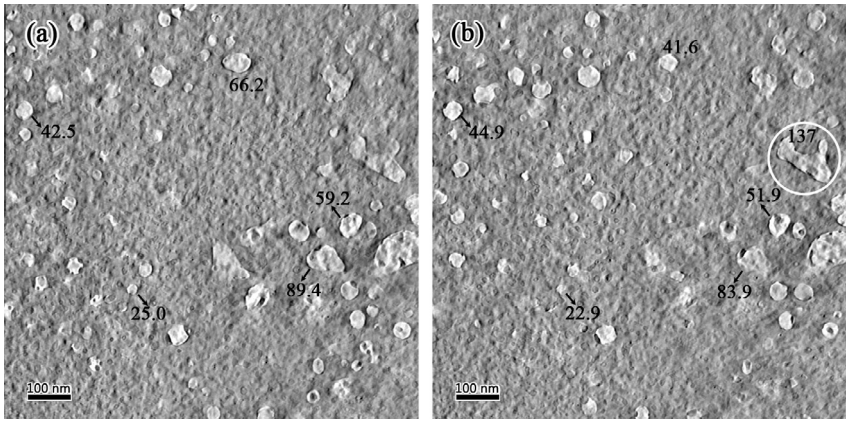

Fig. 4. A z-slice image (a) and an adjacent slice separated by about 10.7 nm (b). The diameters of the circumscribed circles of each pore are shown. Some pores (indicated with a white circle) are especially large in one direction (b).

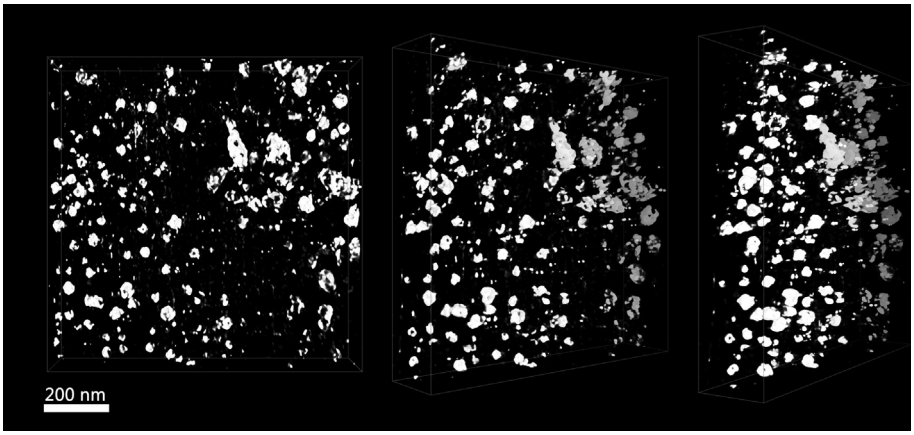

Fig. 6. Three-dimensional renderings of reconstructed tomogram of the geopolymer lamella under different viewing angles clearly showing the irregular shape of the pores in the sample.

et al. [14] showed that large pores upwards of a few hundred of nm coexist with the predominant size ranging from micron to less than 5 nm, and the size of pores ranges from 100 nm to 10 nm. The results presented in Fig. 5 are direct visual observational evidence of fine pores and support their propositions.

Artifacts with a much smaller sized wormhole structure than the pores were generated from the scattering noise of the small disordered zeolite crystals present in the lamella. In bright field electron tomography, the typical algorithms for reconstruction are filtered back projection (FBP) and simultaneous iterative reconstruction technique (SIRT) and both algorithms are not free from artifacts in the reconstruction when crystalline particles are imaged [37]. However, Xu et al. claims that conventional bright field tomography is applicable for tomographic reconstruction of nanoparticles of constant composition, in spite of obvious artifacts, for crystalline particles in the comparative research of reconstruction of polyhedral nanoparticles by bright field TEM and annular dark field specific TEM (STEM) [38]. The spatial distribution of dark patches in crystals seems to be cancelled out over the reconstruction of the whole tilt series [38]. Therefore the wormhole structure is presumably formed by the combined effects of the intensity error, which is caused by Bragg scattering, and non-homogeneous chemical composition of the solid regions. However, these artifacts did not severely distort visual detail such as the shape or size of the pores in the z-slice images (Fig. 4) or in the reconstructed three-dimensional image (Fig. 6). Therefore, the pore size data is believed to be reliable. As shown in Fig. 6, most of pores were not connected and some large pores appeared to have formed by the amalgamation of several adjacent smaller pores. In the three-dimensional tomogram the irregular geometry of the pores was observed to be consistent with that observed in the z-slice images (Fig. 6). As pointed out previously [38,39], the annular dark field scanning transmission electron microscopy (ADF-STEM) reconstruction seems to be more preferable for studying geopolymers, but it should be noted that ADF-STEM tomography has less benefit with lower resolution up to less than one-fifth of the bright field mode [38]. Smaller pores than those identified in this study could be revealed by conducting higher resolution TEM tomography.

Meanwhile, Biermans et al. claims that the effect of the missing wedge causes a decrease of porosity both for manual segmentation and thresholding of the SIRT reconstruction [33]. Missing wedge effect is caused by the limitation of tilt angles up to ±70° and results in artifacts due to the lack of projections in the three-dimensional reconstruction [19,20,40,41]. The porosity value can change if a sample is tilted over ±90° so that the missing wedge effect is completely avoided. Nevertheless, the porosity value obtained in this study is indisputably the first ever three-dimensional quantitative evaluation of fine pores in a geopolymer gel and offers a platform to better understand the pore structure of geopolymers at the nanometer level of spatial resolution.

Abell et al. [10] pointed out that no single technique is able to characterize the complete pore size range in a sample. The results presented in this paper demonstrate that electron tomography provides direct information about the three-dimensional pore network or pore connectivity of geopolymers at the nanometer resolution, which is not readily achieved by X-ray tomography.

4. Conclusions

Conventional bright field electron tomography has been shown to be applicable for the characterization of the pore structure in geopolymers at the nanometer level. This study has provided the first three-dimensional pore shape and distribution data of a geopolymer at the nanoscale by conventional bright field electron tomography in a TEM, which is not achievable using X-ray tomography. The majority of equivalent perimeter diameters of pores in the geopolymer lamella ranged from 20 to 60 nm for 145 pores in four z-slices. Most of the pores did not appear to be connected and they had irregular geometry. The porosity was determined to be 7.15% for the volume of interest, 0.00748 μm^3, which is lower than the values reported in the literature. The data presented in this study provide a platform for better understanding of the geopolymer gel pores at the nanoscale and hopefully, will contribute to the predictions of durability in the future. It is proposed that even higher resolution tomography may be needed to determine if the visualized pores are connected.

Acknowledgments

This study was supported by the Korea Institute of Ocean Science and Technology (Grant No. PE98977) and the R&D Center for Valuable Recycling (Global-Top Environmental Technology Development Program) funded by the Ministry of Environment (Project No.: GT-11-C-01-280-0) in South Korea. We thank Dr. Kweon, Hee-Seok at the Korea Basic Science Institute for the help in the preparation of TEM specimens.

References

[1] Shi C, Jiménez F, Palomo A. New cements for the 21st century: the pursuit of an alternative to Portland cement. Cem Concr Res 2011;41:750–63.
[2] Hughes C. Pore structure and permeability of hardened cement paste. Mag Concr Res 1985;37:27–233.
[3] Scrivenger KL, Bentur A, Pratt PL. Quantitative characterization of the transition zone in high strength concretes. Adv Cem Res 1988;1:230–7.

[4] Mitsui K, Li A, Lange DA, Shah SP. Relationship between microstructure and mechanical properties of the paste-aggregate interface. ACI Mater J 1994;91:30–9.
[5] Scherer GW. Crystallization in pores. Cem Concr Res 1999;29:1347–58.
[6] Diamond S. Aspects of concrete porosity revisited. Cem Concr Res 1999;29:1181–8.
[7] Das BB, Kondraivendhan B. Implication of pore size distribution parameters on compressive strength, permeability and hydraulic diffusivity of concrete. Constr Build Mater 2012;28:382–6.
[8] Jennings HM, Thomas JJ, Gevrenov JS, Constantinides G, Ulm FJ. A multi-technique investigation of the nanoporosity of cement paste. Cem Concr Res 2007;37:329–36.
[9] Rattanasak U, Kendall K. Pore structure of cement/pozzolan composites by X-ray microtomography. Cem Concr Res 2005;35:637–40.
[10] Abell AB, Willis KL, Lange DA. Mercury intrusion porosimetry and image analysis of cement based materials. J Colloid Interface Sci 1999;211:39–44.
[11] Diamond S, Landis EN. Microstructural features of a mortar as seen by computed microtomography. Mater Struct 2007;40:989–93.
[12] Sugiyama T, Promentilla MAB, Hitomi T, Takeda N. Application of synchrotron microtomography for pore structure characterization of deteriorated cementitious materials due to leaching. Cem Concr Res 2010;40:1265–70.
[13] Ma Y, Hu J, Ye G. The pore structure and permeability of alkali activated fly ash. Fuel 2013;104:771–80.
[14] Duxson P, Provis JL, Lukey GC, Mallicoat SW, Kriven WM, van Deventer JSJ. Understanding the relationship between geopolymer composition, microstructure and mechanical properties. Colloids Surf A: Physicochem Eng Aspects 2005;269:47–58.
[15] Kong DLY, Sanjayan JG, Sagoe-Crentsil K. Comparative performance of geopolymers made with metakaolin and fly ash after exposure to elevated temperatures. Cem Concr Res 2007;37:1583–9.
[16] Lange DA, Jennings HM, Shah SP. Image analysis techniques for characterization of pore structure of cement-based materials. Cem Concr Res 1994;24:841–53.
[17] Provis JL, Rose V, Winarski RP, van Deventer JSJ. Hard X-ray nanotomography of amorphous aluminosilicate cements. Scripta Mater 2011;65:316–9.
[18] Provis JL, Myers RJ, White CE, Rose V, van Deventer JSJ. X-ray microtomography shows pore structure and tortuosity in alkali-activated binders. Cem Concr Res 2012;42:855–64.
[19] Ziese U, de Jong KP, Koster AJ. Electron tomography: a tool for 3D structural probing of heterogeneous catalysts at the nanometer scale. Appl Catal A: General 2004;260:71–4.
[20] Midgley PA, Ward EPW, Hungria AB, Thomas JM. Nanotomography in the chemical, biological and materials sciences. Chem Soc Rev 2007;36:1477–94.
[21] Langley WS, Carette GG, Malhotra VM. Structural concrete incorporating high volumes of ASTM Class F fly ash. ACI Mater J 1989;85:507–14.
[22] Lee S, Seo M-D, Kim Y-J, Park H-H, Kim T-N, Hwang Y, et al. Unburned carbon removal effect on compressive strength development in a honeycomb briquette ash-based geopolymer. Int J Miner Process 2010;97:20–5.
[23] van Riessen A, Ghen-Tan N. Beneficiation of Collie fly ash for synthesis of geopolymer: Part 1 – beneficiation. Fuel 2013;106:569–75.
[24] Badanoiu A, Voicu G. Influence of raw materials characteristics and processing parameters on the strength of geopolymer cements based on fly ash. Environ Eng Manage J 2011;10:673–81.
[25] Williams RP, van Riessen A. Determination of the reactive component of fly ashes for geopolymer production using XRF and XRD. Fuel 2010;89:3683–92.
[26] Diez DC, Seybert A, Frangakis AC. Tilt-series and electron microscope alignment for the correction of the non-perpendicularity of beam and tilt-axis. J Struct Biol 2006;154:195–205.
[27] Jou H-T, Lee S, Kim H-J. Improvement of alignment accuracy in electron tomography. Appl Microsc 2013;43:1–8.
[28] Gilbert PFC. The reconstruction of a three-dimensional structure from projections and its application to electron microscopy. II. Direct methods. Proc Roy Soc London. Ser B – Biol Sci 1972;182:89–102.
[29] Lloyd RR, Provis JL, van Deventer JSJ. Microscopy and microanalysis of inorganic polymer cements. J Mater Sci 2009;44:620–31.
[30] Rees CA, Provis JL, Lukey GC, van Deventer JSJ. Attenuated total reflectance fourier transform infrared analysis of fly ash geopolymer gel aging. Langmuir 2007;23:8170–9.
[31] van Deventer JSJ, Provis JL, Duxson P. Technical and commercial progress in the adoption of geopolymer cement. Miner Eng 2012;29:89–104.
[32] Komljenović M, Baš č arević Z, Bradić V. Mechanical and microstructural properties of alkali-activated fly ash geopolymers. J Hazard Mater 2010;181:35–42.
[33] Biermans E, Molina L, Batenburg KJ, Bals S, van Tendeloo G. Measuring porosity at the nanoscale by quantitative electron tomography. Nano Lett 2010;10:5014–9.
[34] Landis EN, Keane DK. X-ray microtomography. Maters Charact 2010;61:1305–16.
[35] Lloyd RR, Provis JL, Smeaton KJ, van Deventer JSJ. Spatial distribution of pores in fly ash-based inorganic polymer gels visualized by Wood's metal intrusion. Microporous Mesoporous Mater 2009;126:32–9.
[36] Kriven WM, Bell JL, Gordon M. Microstructure and microchemistry of fully-reacted geopolymers and geopolymer matrix composites. Ceram Trans 2003;153:227–50.
[37] Venkatakrishnan SV, Drummy LF, De Graef M, Simmons JP, Bouman CA. Model based iterative reconstruction for bright field electron tomography. In: Proc. SPIE 8657, Computational Imaging XI, Burlingame, California, USA, February 03, 2013.
[38] Xu X, Saghi Z, Gay R, Möbus G. Reconstruction of 3D morphology of polyhedral nanoparticles. Nanotechnology 2007;18:225501 (8pp).
[39] Möbus G, Inkson BJ. Nanoscale tomography in materials science. Mater Today 2007;10:18–25.
[40] Koster AJ, Ziese U, Verkleij AJ, Janssen AH, de Jong KP. Three-dimensional transmission electron microscopy: a novel imaging and characterization technique with nanometer scale resolution for materials science. J Phys Chem B 2000;104:9368–70.
[41] Weyland M, Midgley P. Electron tomography. Mater Today 2004;7:1.